Energy diffusion in two-dimensional momentum-conserving nonlinear lattices: Lévy walk and renormalized phonon

Yanjiang Guo (郭彦江), Yachao Sun (孙亚超), and Lei Wang (王雷)*
Department of Physics and Beijing Key Laboratory of Opto-electronic Functional Materials and Micro-nano Devices, Renmin University of China, Beijing 100872, People's Republic of China

(Received 28 May 2022; accepted 21 December 2022; published 10 January 2023)

The energy diffusion process in a few two-dimensional Fermi-Pasta-Ulam-type lattices is numerically simulated via the equilibrium local energy spatiotemporal correlation. Just as the nonlinear fluctuating hydrodynamic theory suggested, the diffusion propagator consists of a bell-shaped central heat mode and a sound mode extending with a constant speed. The profiles of the heat and sound modes satisfy the scaling properties from a random-walk-with-velocity-fluctuation process very well. An effective phonon approach is proposed, which expects the frequencies of renormalized phonons as well as the sound speed with quite good accuracy. Since many existing analytical and numerical studies indicate that heat conduction in such two-dimensional momentum-conserving lattices is divergent and the thermal conductivity κ increases logarithmically with lattice length, it is expected that the mean-square displacement of energy diffusion grows as $t \ln t$. Discrepancies, however, are noticeably observed.

DOI: 10.1103/PhysRevE.107.014109

I. INTRODUCTION

The continuous-time random walk (CTRW) formalism has found applications in a wide range of phenomena. In particular, the Lévy walk (LW) approach [1] has been successfully applied for the description of superdiffusion in various physical systems, e.g., particle diffusion in a one-dimensional (1D) dynamical channel [2], in a two-dimensional (2D) rotating flow [3], in 1D and 2D optical molasses derived from counterpropagating laser beams, and also energy diffusion in many-particle Hamiltonian systems [4,5]. On the other hand, through a few decades' in-depth studies, a consensus has been commonly reached that heat conduction in a 1D momentum-conserving nonlinear system is generally anomalous [6]. Mode-coupling theory [7] and renormalization group analysis [8] both suggest that the global heat current autocorrelation $C_{JJ}(t)$ decays as $t^{-\gamma}$ with $\gamma < 1$, thus according to the Green-Kubo formula [9] the corresponding heat conductivity κ diverges with the system size L as $\kappa \sim L^{\alpha}$ with $0 < \alpha < 1$. Such a power-law divergence was first revealed in a 1D Fermi-Pasta-Ulam (FPU) lattice [10] and later has been observed in various 1D nonlinear systems [11–14]. Very recently, a stochastic fractional diffusion equation which confirms the anomalous transport in a linear system with stochastic momentum exchange has been proposed [15]. Correspondingly, energy diffusion in such systems is generally superdiffusive [16]. According to the nonlinear fluctuating hydrodynamic theory [17], the diffusion propagator [18] consists of a bell-shaped central heat mode and two sound modes moving out in opposite directions with a constant sound speed v_s. The mean-square displacement (MSD) of the propagator follows a power-law divergence $\sigma^2(t) \sim t^{\beta}$ with $\beta > 1$, and more importantly the evolution of the propagator can be well described by a LW [4,5,19]. A general relation $\frac{d^2}{dt^2}\sigma^2(t) = \frac{2C_{JJ}(t)}{k_B T^2 c_v}$ where c_v denotes the specific volumetric heat capacity connects the two power exponents α and β by $\beta = \alpha + 1$ [20].

These properties are certainly dimension dependent. For 2D momentum-conserving nonlinear systems, the mode-coupling theory and renormalization group analysis also suggest that $C_{JJ}(t)$ decays as t^{-1}, thus the corresponding heat conductivity κ diverges logarithmically. Such a t^{-1} decay of $C_{JJ}(t)$ and a logarithmic divergence of κ have been observed in FPU-β rectangle [21] and disk [22] lattices with vector displacements and a 2D purely quartic rectangle lattice with scalar displacements [23]. Consequently, the MSD of the diffusion propagator, according to the above-mentioned general relation, should follow $\sigma^2(t) \sim t \ln t$ in the long t limit. In contrast to the extensive studies of the 1D systems, very few studies of the energy diffusion process in 2D nonlinear lattices have been done due to great difficulties in both theoretical analyses and numerical simulations [19]. The $t \ln t$ divergence has not been convincingly checked, and more importantly, whether the detailed diffusion process can be described within the LW framework has not been clearly investigated either.

In this paper, the energy diffusion process in a few 2D FPU-type nonlinear lattices is investigated systematically via numerical simulations. Heat and sound modes are both observed clearly. Furthermore, for each lattice, the scalings of the central part of the heat mode, the decay of its tail, and possibly also the decay of the sound mode are all governed by a single parameter, the decay power exponent of the duration time τ of each walk in a LW, if the energy carriers are regarded as the walkers. We then extend a renormalized phonon approach to 2D and found that the numerically measured sound speed agrees very well with its expectation. Finally, the above-mentioned general connection between the superdiffusion and

*phywanglei@ruc.edu.cn

divergent heat conduction is checked but noticeable discrepancies are observed. The paper is organized as follows. The 2D lattice models and spatiotemporal correlation of the local energy density are introduced in Sec. II. The results of a detailed numerical simulation and the corresponding theoretical analyses are presented in Sec. III. A summary and discussion are provided in Sec. IV.

II. MODEL AND SIMULATION

A. Two-dimensional momentum-conserving nonlinear lattices

We study energy diffusion in a few 2D square lattices with a scalar displacement field $u_{i,j}$. Each particle interacts with its nearest neighbors. The Hamiltonian of the system with $N = N_X \times N_Y$ particles reads

$$H = \sum_{i=1}^{N_X}\sum_{j=1}^{N_Y}\left[\frac{\dot{u}_{i,j}^2}{2} + V(\Delta x_{i,j}) + V(\Delta y_{i,j})\right], \tag{1}$$

where $\Delta x_{i,j} \equiv u_{i,j} - u_{i-1,j}$, $\Delta y_{i,j} \equiv u_{i,j} - u_{i,j-1}$, and the interparticle potential takes a FPU form

$$V(q) = \tfrac{1}{2}Kq^2 + \tfrac{1}{4}\lambda q^4. \tag{2}$$

The masses of all the particles have been set to unity. Periodic boundary conditions are always applied, i.e., $u_{0,j} \equiv u_{N_X,j}$ and $u_{i,0} \equiv u_{i,N_Y}$. We choose the scalar displacement, i.e., each particle can move only in 1D space. Our study will focus on the role of the linear part of the interaction, thus the nonlinear term λ has been fixed to unity and four values of the linear strength $K = 0$, 0.2, 0.5 and 1, will be studied. When $K = 0$, the lattice reduces to a purely quartic (PQ) lattice, and when $K = 1$, the lattice is a standard FPU-β lattice. The PQ lattice can be regarded as the high-temperature or strong-nonlinearity limit of the FPU-type lattices. Commonly its asymptotic behaviors could be displayed in shorter timescales and space scales. Unless otherwise stated, the PQ and the FPU-β lattices refer to these two types hereafter and much more attention will be paid to them. We study only a symmetric interaction $[V(q) = V(-q)]$ so that there is no temperature pressure, no particle flow, and no work.

B. Spatiotemporal correlation of local energy density

The spatiotemporal correlation of the local energy density provides a quite efficient way of characterizing the diffusion propagator via equilibrium simulation [24]. It can be directly applied in 2D cases. In an equilibrium state, the spatiotemporal correlation function of the local energy density is defined as

$$C_{\mathrm{EE}}(i, j, t) \equiv \langle \Delta E_{ij}(t)\Delta E_{00}(0)\rangle, \tag{3}$$

where $\Delta E_{ij}(t) \equiv E_{ij}(t) - \langle E_{ij}\rangle$ is the excess local energy density. The local energy is defined naturally as

$$E_{ij}(t) \equiv \frac{\dot{u}_{i,j}^2}{2} + \frac{1}{2}[V(\Delta x_{i,j}) + V(\Delta x_{i+1,j}) + V(\Delta y_{i,j}) + V(\Delta y_{i,j+1})]. \tag{4}$$

In a homogeneous lattice, $\langle E_{ij}\rangle$ is site independent and is simply equal to $\langle E\rangle$, the per-particle average energy. To remove an inherent correlation that is induced by energy conservation, the rescaled local energy correlation function, which is equivalent to the diffusion propagator [25], is defined as [26]

$$\rho_{\mathrm{E}}(i, j, t) \equiv \frac{C_{\mathrm{EE}}(i, j, t)}{\sum_{|i|+|j|\leqslant 1} C_{\mathrm{EE}}(i, j, 0)} + \frac{1}{N-5}. \tag{5}$$

The MSD of $\rho_{\mathrm{E}}(i, j, t)$ reads

$$\sigma^2(t) \equiv \sum_{i,j}(i^2 + j^2)\rho_E(i, j, t), \tag{6}$$

which characterizes the MSD of the energy diffusion propagator.

III. NUMERICAL RESULTS AND ANALYSES

A. Overall distribution profile

Microcanonical simulations are performed in lattices with zero total momentum, all zero initial displacements, and an identical average energy density ϵ which corresponds to a fixed temperature $T = 1$. Averages are taken over more than 10^6 time units and the system size is 501×501.

To have a global picture of the diffusion process, we first plot the snapshots of $\rho_{\mathrm{E}}(i, j, t)$ at $t = 160$ for the FPU-β and PQ lattices in Figs. 1(a) and 1(b), respectively. In order to reduce the statistical fluctuation, based on the XY and reflection symmetries, we plot actually not the $\rho_{\mathrm{E}}(i, j, t)$ itself but

$$\begin{aligned}\rho'_{\mathrm{E}}(i, j, t) \equiv \tfrac{1}{8}[&\rho_{\mathrm{E}}(i, j, t) + \rho_{\mathrm{E}}(-i, j, t) + \rho_{\mathrm{E}}(i, -j, t)\\ &+ \rho_{\mathrm{E}}(-i, -j, t) + \rho_{\mathrm{E}}(j, i, t) + \rho_{\mathrm{E}}(-j, i, t)\\ &+ \rho_{\mathrm{E}}(j, -i, t) + \rho_{\mathrm{E}}(-j, -i, t)]\end{aligned} \tag{7}$$

instead. We see a quite clear central peak and a circle with a radius about 200 and 170 around the origin. They correspond to the heat and sound modes of the energy diffusion. Interestingly, we see that the sound mode displays a double ring.

In order to observe the details of the diffusion more clearly, we plot the cross section at the axis, i.e., $\rho'_{\mathrm{E}}(i, 0, t)$ or $\rho'_{\mathrm{E}}(0, j, t)$ in Figs. 1(c) and 1(d). The sound modes are much lower than those in the 1D lattices [19,27]. Corresponding to the double ring observed in the 2D profile, the cross section of the sound mode displays a double peak, which is not observed in 1D FPU-type lattices.

B. Scaling properties of the heat mode

1. Return probability and scaling of the central part

It is predicted by the nonlinear fluctuating hydrodynamic theory [17] that for a 1D model with three conserved quantities—energy, momentum, and stretch—a small perturbation will induce a central bell-shaped heat mode and two sound modes moving out in opposite directions with a constant speed v_s. The tail of the heat mode is cut at the location of the sound mode. On the other hand, a LW describes a walker moving with a constant velocity v_0 and direction for a random time τ and then, at a turning point, instantaneously choosing a new direction and moving again [28]. There exists a ballistic cone extending with the velocity, beyond which no walker can go. Due to the similarity of the underlying mechanisms and also the distribution properties of the above two processes, one naturally tries to describe the energy diffusion process

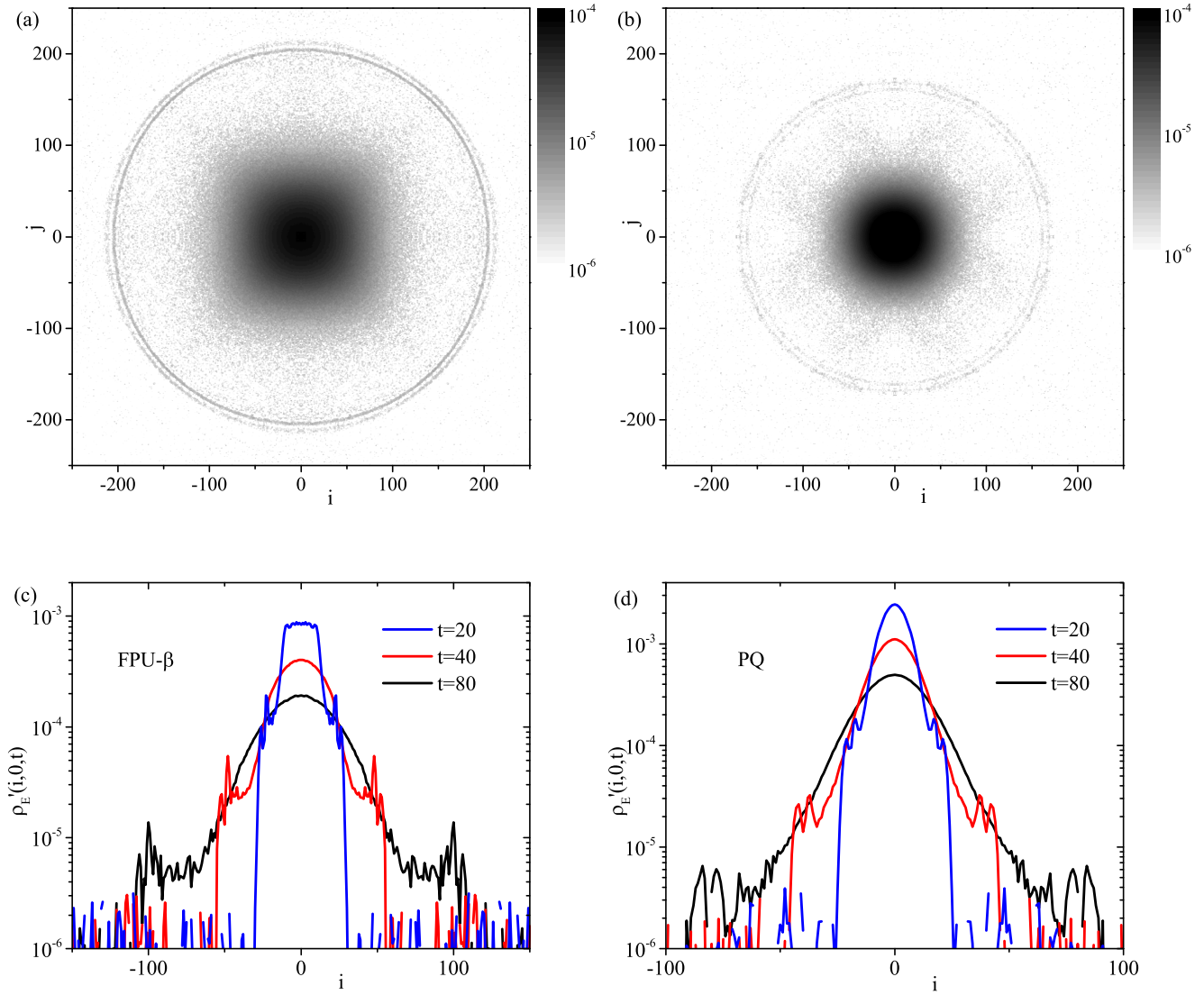

FIG. 1. Snapshots of the rescaled local energy correlation $\rho'_{\mathrm{E}}(i, j, t)$ at time $t = 160$ for (a) the FPU-β lattice and (b) the PQ lattice. Clear circles with radii about 200 and 170 can be observed respectively for the two lattices. (c) and (d) 1D distributions of the two lattices in a single logarithmic plot. The curves from the top down are for $t = 20$, 40, and 80. Small peaks that correspond to the above-mentioned circles can be observed.

phenomenologically by a LW, although LW commonly describes the motions of real objects. In such a case, the energy carriers, possibly the effective phonons [29], are regarded as the "walkers" of the LW.

Suppose the duration time τ of each move of LW is independent and follows an identical distribution $\psi(\tau)$ that satisfies a power-law decay [4,5]

$$\psi(\tau) = \left(\frac{\tau}{\tau_0}\right)^{-\mu-1}, \tag{8}$$

then in the long-time t cases the central part of the probability density function (PDF) of the walkers of LW is governed by a Lévy stable distribution

$$\rho_{1\mathrm{D}}(x, t) \sim P_L(x, t) = \frac{1}{\pi}\int_0^\infty e^{-\eta t z^\mu}\cos(zx)dz, \tag{9}$$

where μ is the index of the Lévy distribution and $\eta \sim v_0^\mu \tau_0{}^{\mu-1}$ describes the speed of diffusion. Throughout this paper, only the superdiffusion regime, i.e., $\mu \in (1, 2)$, will be studied. $\rho_{1\mathrm{D}}(x, t)$ is a bell-shaped distribution with height

$$\rho_{1\mathrm{D}}(0, t) = \frac{1}{\pi}\int_0^\infty e^{-\eta t z^\mu} dz = \frac{\Gamma\left(\frac{1}{\mu}\right)\eta^{-\frac{1}{\mu}} t^{-\frac{1}{\mu}}}{\mu\pi}, \tag{10}$$

which decays with time t by $t^{-\frac{1}{\mu}}$. The Γ function $\Gamma(x) \equiv \int_0^\infty t^{x-1}e^{-t}dt$. $\rho_{1\mathrm{D}}(x, t)$ satisfies a scaling invariant relation

$$\rho_{1\mathrm{D}}(x, ut) \sim u^{-\frac{1}{\mu}}\rho_{1\mathrm{D}}(u^{-\frac{1}{\mu}}x, t). \tag{11}$$

For ballistic and normal diffusion, $\mu = 1$ and 2, respectively, and values in between correspond to superdiffusion. Such a scaling has been observed in various 1D systems [4,5,19].

To extend the LW to 2D, various intuitive methods are available [30], including the so-called product model where

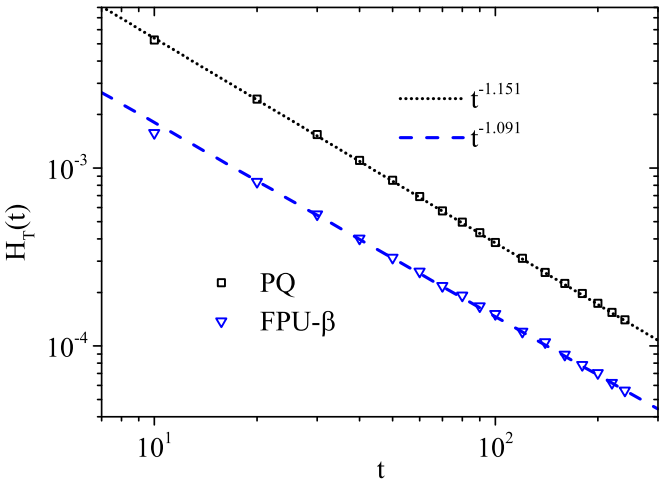

FIG. 2. The height of the heat mode $H_T(t) = \rho_E(0, 0, t)$ vs time t for the 2D PQ (black squares) and FPU-β (blue triangles) lattices. Lines with the best fitted slopes -1.151 and -1.091 are plotted for reference.

the motions along each axis are identical 1D LW processes, the so-called XY model where the walkers choose each step of LW along one of the X or Y directions with equal probability, and the so-called uniform model where each step a walker chooses a random direction from a uniform distribution. Based on the observed nearly isotropic distributions shown in Figs. 1(a) and 1(b), the uniform model might be the best choice. As a result, the scaling relation in 2D follows

$$\rho_{2D}(x, 0, ut) \sim u^{-\frac{2}{\mu}} \rho_{2D}(u^{-\frac{1}{\mu}} x, 0, t), \tag{12}$$

and $\mu = 2$ is still the border that separates normal diffusion and superdiffusion. The height of the heat mode $H_T(t) = \rho_E(0, 0, t)$ in the 2D lattices is then expected to decay with t by $t^{-\frac{2}{\mu}}$. In Fig. 2, $H_T(t)$ versus time t for the 2D FPU-β and PQ lattices are plotted in double logarithmic scale. The data follow straight lines very well. The scaling power exponents can thus be determined very exactly. The best fitted slope for the last 15 points of the FPU-β lattice reads -1.091 ± 0.005 and that for the last 16 points of the PQ lattice reads -1.151 ± 0.002. Correspondingly, $\mu = 1.834$ and 1.738 for the FPU-β and PQ lattices, respectively. The diffusion in the observed time regime is slightly, however evidently, faster than normal in both lattices.

To check the 2D scaling relation Eq. (12), we plot the rescaled distribution $t^{\frac{2}{\mu}} \rho'_E(i, t)$ vs $it^{-\frac{1}{\mu}}$ for the 2D FPU-β and PQ lattices in Figs. 3(a) and 3(b), respectively. For the FPU-β lattice all the data for different times t overlap each other very well, except for the very short time $t = 20$ (black squares) and 40 (red circles) cases. For the PQ lattice, the overlap is even better. The validity of the scaling Eq. (12) is then strongly confirmed.

2. Decay of the tail

In the large $|x|$ cases the Lévy stable distribution Eq. (9) follows asymptotically,

$$\rho_{1D}(x, t) \sim \frac{\eta \Gamma(\mu + 1) \sin\left(\frac{\pi\mu}{2}\right)}{\pi} t |x|^{-(\mu+1)}. \tag{13}$$

The tail decays asymptotically as $|x|^{-(\mu+1)}$ [31]. Such a fat tail, which induces a divergent second moment, is a key feature of the Lévy distribution. The PDF of a LW should satisfy this scaling in the regime $|x| \in (\eta^{1/\mu} t^{1/\mu}, v_s t)$ [32].

For 2D LW, the distribution $\rho_{2D}(x, y, t)$ might be quite complicated [30]. Due to its rotation invariance, in the large radius $r \equiv \sqrt{x^2 + y^2}$ regime, the radial distribution should be a Lévy with the same index μ. Therefore, the tail of $\rho_{2D}(r, t)$ should decay as

$$\rho_{2D}(r, t) \sim C t r^{-(\mu+2)}, \tag{14}$$

which still implies a well-defined mean value but a divergent second moment. The decay exponent $-(\mu + 2)$ equals -3.834 and -3.738 for the 2D FPU-β and PQ lattices, respectively. In Figs. 3(c) and 3(d), we plot the rescaled tail distributions for the two 2D lattices as well as the curves that satisfy the power law $i^{-(\mu+2)}$ in double logarithmic scale. We see that the curves for different t basically overlap each other in a regime, in which the power-law decays basically follow the above expectations [Eq. (14)]. As a conclusion, the LW describes quite well the superdiffusion of the heat mode in these 2D lattices.

C. Scaling and speed of the sound mode

1. Scaling of the sound mode

Next, we turn to the profile of the sound mode. For 1D systems, the original LW approach failed to capture the dynamics of the sound modes [4] since they display smooth, humplike profiles, and with a scaling that was incompatible with the scaling behavior of the delta-function-like peaks of the LW propagator [5]. Therefore, the interaction between the walkers, which causes fluctuations of their velocities, must be considered. The diffusion process is then characterized by a random-walk-with-velocity-fluctuation process [28], during which the dispersion of the humplike sound mode grows as $t^{\frac{1}{2}}$ and the volume of the sound mode generally follows a power-law decay $t^{-\xi}$. Then the height of the sound mode $H_S(t)$ decays as $t^{-(\xi+\frac{1}{2})}$ and its PDF satisfies the scaling [5]

$$\rho_{1D\ \mathrm{sound}}(\bar{x}, ut) \sim u^{-(\xi+\frac{1}{2})} \rho_{1D\ \mathrm{sound}}(u^{-\frac{1}{2}} \bar{x}, t), \tag{15}$$

where $\bar{x} \equiv x - v_s t$ and v_s is the speed of sound. In 2D cases, supposing again the radial diffusion is described by a LW and the decay of volume and the growth of dispersion remain unchanged, since the sound mode forms a circle whose radius is proportional to time t, $H_S(t)$ should decay with t by not $t^{-(\xi+\frac{1}{2})}$ but $t^{-(\xi+\frac{3}{2})}$, and the scaling of the PDF should change to

$$\rho_{2D\ \mathrm{sound}}(\bar{x}, ut) \sim u^{-(\xi+\frac{3}{2})} \rho_{2D\ \mathrm{sound}}(u^{-\frac{1}{2}} \bar{x}, t). \tag{16}$$

The detailed value of ξ may vary and depend on the memory effect of the system [28]. For the so-called equilibrated setup where we suppose that the system has reached a certain equilibrium before we start measuring it, $\xi = \mu - 1$ [5,32], whereas for the nonequilibrated setup where all walkers are introduced to the system at $t = 0$ and do not have prehistories, $\xi = \mu$ [32]. Since μ equals 1.834 and 1.738 for the 2D FPU-β and PQ lattices, respectively, the expected power exponent $-(\xi + \frac{3}{2})$ equals -2.334 and -2.238 for the equilibrated

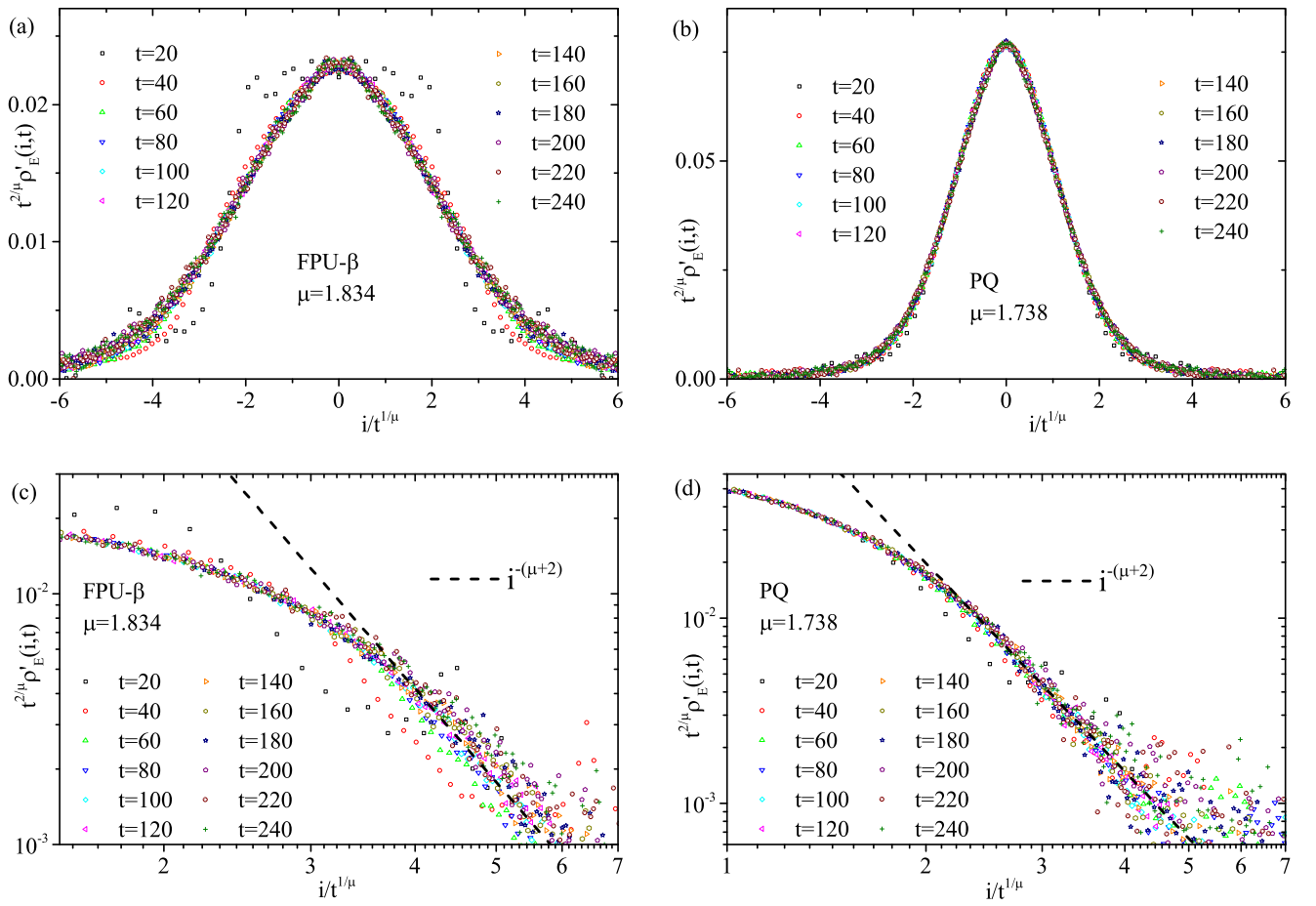

FIG. 3. The rescaled central distribution of (a) the FPU-β and (b) the PQ lattices in linear scale. (c) and (d) The rescaled tail distributions of the two lattices in double logarithmic scale.

setup, and -3.334 and -3.238 for the nonequilibrated setup. In our system, the walkers (phonons) do have their own prehistories and different ages at $t = 0$, thus the former scaling is naturally expected. The simulations also prefer it. In Fig. 4(a), the height of the sound mode $H_S(t)$ versus time t for $t \leqslant 90$ as well as the above predicted power-law decays are plotted. Due to the very fast decay of the sound mode, it is hard to determine $H_S(t)$ for even longer t. Therefore, we are not able to draw a very convincing conclusion for the long t limit. Nevertheless, we can see that the data in the plotted regime prefer the former one, i.e., the equilibrated setup where $\xi = \mu - 1$. In Figs. 4(b) and 4(c), we plot the rescaled correlations according to the equilibrated setup versus the rescaled coordinate $(i - v_s t)t^{-\frac{1}{2}}$. The speed of sound v_s equals 1.325 and 1.056, respectively, for the FPU-β and PQ lattices. The way to determine v_s will be discussed later in Sec. III C 2. Also due to the very fast decay of the sound mode, fluctuation soon dominates, thus the data for even longer time $t > 80$ cannot display well the overlap. Given the large relative fluctuation, the overlap of the data for various time t in the plotted regime is acceptable, in particular for the PQ lattice. As a comparison, those according to the nonequilibrated setup are also plotted in Figs. 4(d) and 4(e). The overlap is apparently poor. The validity of the random-walk-with-velocity-fluctuation description and also the equilibrated setup in these 2D nonlinear lattices is then confirmed.

It is also observed that, unlike in a general 1D strong nonlinearly lattice that a sound mode forms a single-peak profile, the cross section of the sound mode in these 2D lattices apparently does not. This fact implies that the simple presumption of the interaction is incomplete here. More in-depth studies are necessary to well understand such an unexpected profile.

2. Speed of sound

The LW provides universal connections among various scaling power exponents. However, the absolute value of some key quantities still depends on the details of the system. An important one is the speed of sound v_s, which determines the velocity of the ballistic peaks of the LW. For the lattice models, v_s can be calculated by the group velocity of effective phonons [29].

For a 2D standard linear lattice ($K = 1$ and $\lambda = 0$), the dynamics of the system is described by a linear differential equation group. The dispersion relation is known analytically as

$$\omega_{1,0}(k_x, k_y) = 2\sqrt{\sin^2\frac{k_x\pi}{N_X} + \sin^2\frac{k_y\pi}{N_Y}}, \qquad (17)$$

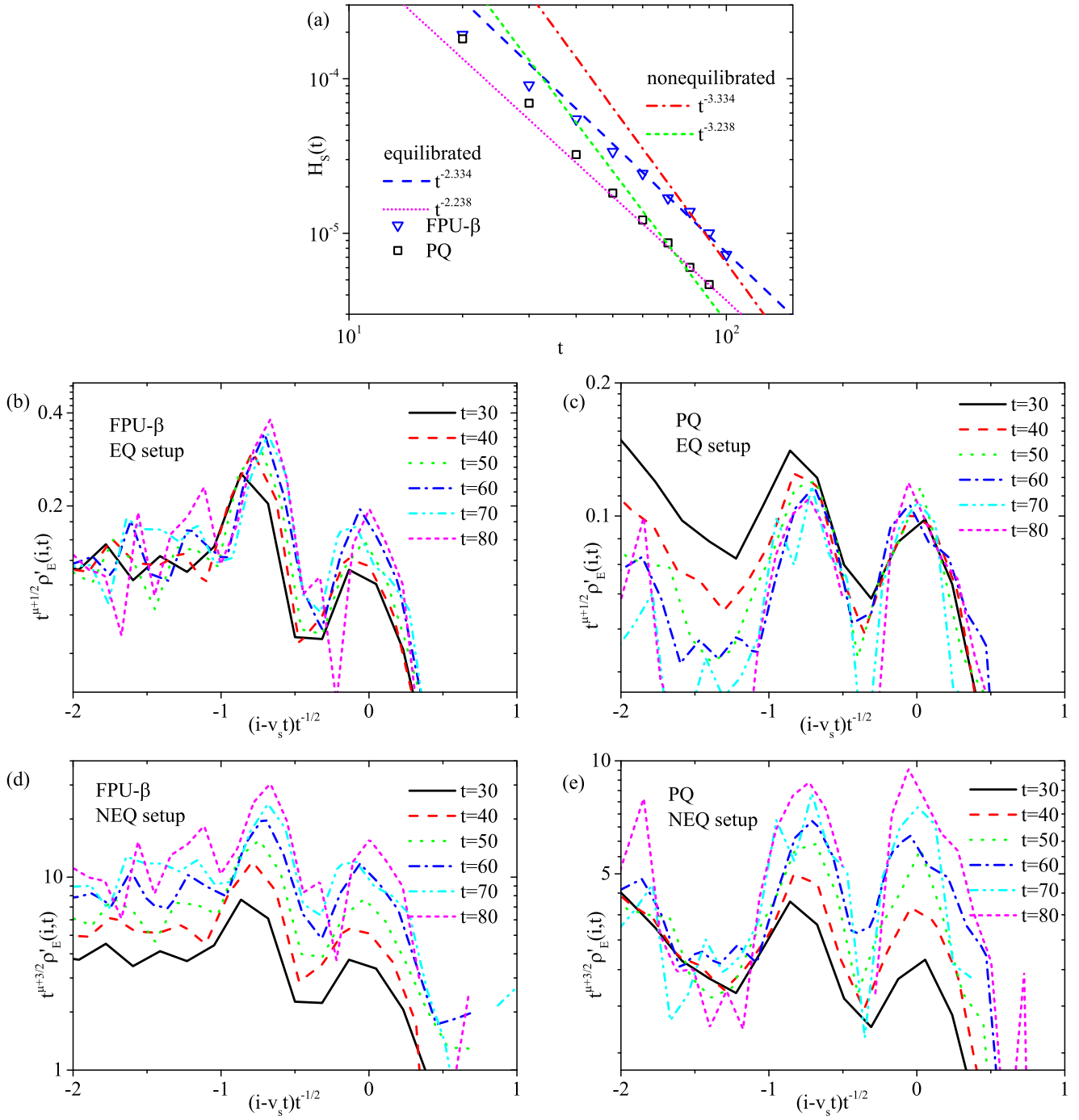

FIG. 4. (a) The height of sound mode $H_S(t)$ vs time t for the 2D FPU-β and PQ lattices. The power-law decays that are predicted by the equilibrated setup $t^{-2.334}$ and $t^{-2.238}$, and by the nonequilibrated setup $t^{-3.334}$ and $t^{-3.238}$ are also plotted for reference. The numerical data follow the equilibrated ones much better. (b) and (c) The rescaled correlation $t^{\mu+\frac{1}{2}}\rho'_E(i,t)$ according to the equilibrated setup vs the rescaled coordinate $(i-v_s t)t^{-\frac{1}{2}}$. In the long t cases, those for different t basically overlap each other. (d) and (e) The rescaled correlation $t^{\mu+\frac{3}{2}}\rho'_E(i,t)$ according to the nonequilibrated setup. The overlap is apparently not as good as those for the equilibrated setup.

where $k_{x/y} = 0, 1, 2, \ldots, N_{X/Y} - 1$. The subscripts of ω denote the values of K and λ. In the thermodynamic limit $N_X, N_Y \to \infty$, Eq. (17) takes a continuous form

$$\tilde{\omega}_{1,0}(k'_x, k'_y) = 2\sqrt{\sin^2\frac{k'_x}{2} + \sin^2\frac{k'_y}{2}}, \tag{18}$$

where $k'_x, k'_y \in [0, 2\pi)$. The speed of sound $v_s(1,0)$ in any direction $(k'_x, k'_y) = (k'\cos\theta, k'\sin\theta)$ equals

$$v_s(1,0) = \left.\frac{\partial\tilde{\omega}_{1,0}(k'_x, k'_y)}{\partial|k'|}\right|_{|k'|\to 0} = 1, \tag{19}$$

which is orientation θ independent. Thus the sound mode forms a circle.

When nonlinearity is present, the motion of the system is still periodiclike [33], but with renormalized phonon frequencies $\omega_{K,\lambda}(k_x, k_y)$ that read

$$\omega_{K,\lambda}(k_x, k_y) = \eta_{2D}(K, \lambda)\omega_{1,0}(k_x, k_y). \tag{20}$$

In an equilibrium state, the renormalization factor $\eta_{2D}(K, \lambda)$ should be mode independent due to the Gibbs measure, as for the cases in 1D [33,34].

For a 1D FPU-type lattice, in which the interparticle potentials take the same form as shown in Eq. (2), the renormalized frequencies

$$\omega_{K,\lambda}(k) = \eta_{1D}(K, \lambda)\omega_{1,0}(k). \tag{21}$$

An estimation suggested via the self-consistent phonon theory (SCPT) [35,36] and the renormalized phonon approach [37] reads

$$\eta_{1D}(K, \lambda) = \sqrt{\frac{K + \sqrt{K^2 + 12\lambda T}}{2}}. \tag{22}$$

This agrees quite well with numerical simulations [37].

Intuitionistically speaking, in a 2D square lattice the potential energy of each particle is shared by not two but four connections. The amount in each connection is thus reduced by half compared with the 1D lattices. As a result, the term temperature T in Eq. (22) should also be divided by 2, i.e.,

$$\eta_{2D}(K, \lambda) = \sqrt{\frac{K + \sqrt{K^2 + 6\lambda T}}{2}}. \tag{23}$$

We will detail a more rigorous derivation of Eq. (23) in the Appendix. Correspondingly, the speed of sound in the 2D nonlinear lattices is expected to be

$$v_s(K, \lambda) = \eta_{2D}(K, \lambda)v_s(1, 0). \tag{24}$$

Since the derivation in Eq. (19) is performed in the long-wavelength limit, we are interested more in the low-frequency regime. In Fig. 5, the power spectra $P(\omega)$ of the lattices with size 501×501 for fixed $\lambda = 1$ and various $K = 0$, 0.2, 0.5, and 1 are plotted. The renormalized frequency $\omega_{K,\lambda}$, i.e., the prediction of Eqs. (17), (20), and (23), of a few lowest-nonzero-frequency modes [38] are also plotted as symbols for reference. $\omega_{K,\lambda}$ agrees quite well with $\omega^{\text{num}}_{K,\lambda}$, which corresponds to the locations of the peaks of $P(\omega)$, with only a few percents' relative overestimation (RO). The greater the K, i.e., the lower the relative nonlinearity, the smaller the overestimation. The detailed values of $\omega^{\text{num}}_{K,\lambda}$ and $\omega_{K,\lambda}$ of the lowest-nonzero-frequency mode for each lattice, as well as the relative overestimation, are listed in Table I, middle group (columns 2–4).

To determine the speed of sound in the lattices numerically, we measure the radius $R_S(t)$ of the sound mode versus time t [39]. $R_S(t)$ for various $K = 0$, 0.2, 0.5, and 1 are plotted in Fig. 5(b). The data follow very good straight lines. The best fitted slopes $v_s^{\text{num}}(K, \lambda)$ are shown in the legend. The comparison of $v_s^{\text{num}}(K, \lambda)$ with their expectations $v_s(K, \lambda)$ is plotted in the inset and also listed in Table I, right-hand group (columns 5–7). The agreement is quite well. The observed

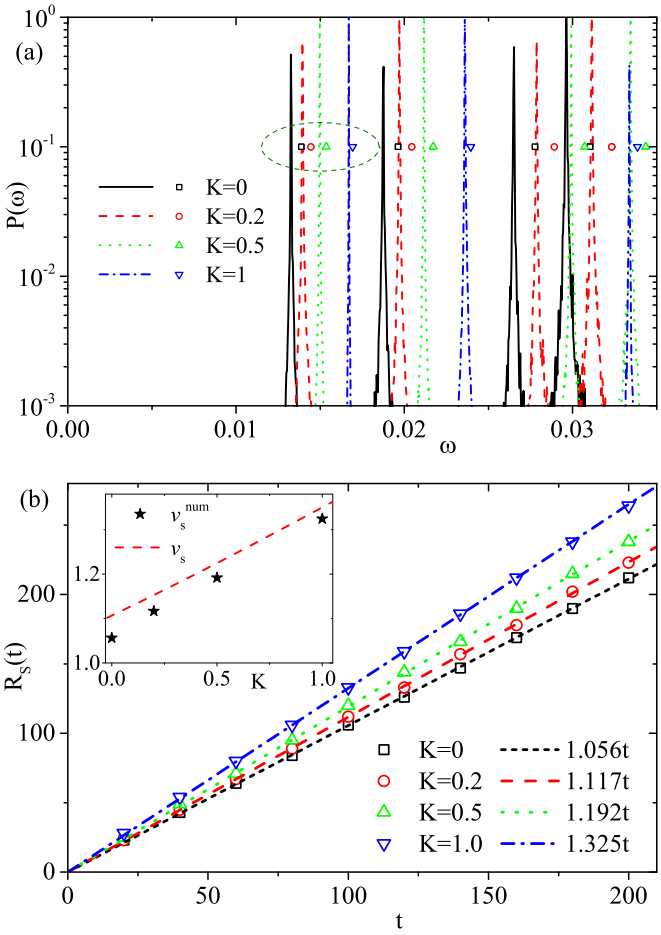

FIG. 5. (a) Power spectra $P(\omega)$ (curves) for lattices with various linear strengths K. System size $N_X = N_Y = 501$. Symbols indicate the locations of a few lowest-nonzero-frequency modes expected by Eqs. (17), (20), and (23). Detailed values of $\omega_{K,\lambda}$ of the lowest-nonzero-frequency modes for each lattice, which are surrounded by the dashed circle, are also listed in Table I. (b) The radius $R_S(t)$ of the sound modes vs time t of 2D lattices with various K (symbols). Lines are their corresponding best linear fits, whose slopes are shown in the legend. Inset: The speed of sound measured by numerical simulation $v_s^{\text{num}}(K, \lambda)$ (black stars) and the analytical expectation $v_s(K, \lambda)$ (red dashed curve), vs linear strength K.

TABLE I. Renormalized phonon frequency and speed of sound for 2D lattices with fixed $\lambda = 1$ and various K. System size $N_X = N_Y = 501$. Middle group (columns 2–4): The frequency of the lowest-nonzero-frequency mode measured numerically $\omega^{\text{num}}_{K,\lambda}$, expected by Eqs. (17), (20), and (23), $\omega_{K,\lambda}$, and the relative overestimation. Right-hand group (columns 5–7): The speed of sound measured numerically $v_s^{\text{num}}(K, \lambda)$, expected by Eq. (24), $v_s(K, \lambda)$, and the relative overestimation.

K	$\omega^{\text{num}}_{K,\lambda}$	$\omega_{K,\lambda}$	RO	$v_s^{\text{num}}(K, \lambda)$	$v_s(K, \lambda)$	RO
0	0.013258	0.013879	4.7%	1.056 ± 0.002	1.107	4.8%
0.2	0.013932	0.014457	3.8%	1.117 ± 0.003	1.153	3.2%
0.5	0.014980	0.015360	2.5%	1.192 ± 0.002	1.225	2.8%
1.0	0.016703	0.016932	1.4%	1.325 ± 0.002	1.350	1.9%

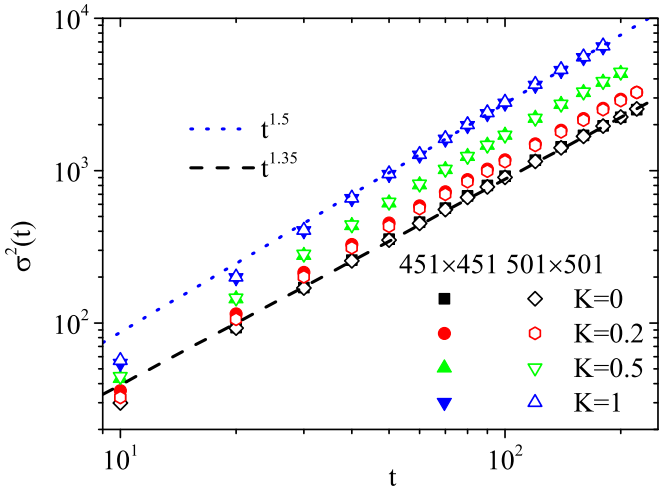

FIG. 6. The MSD of the diffusion $\sigma^2(t)$ vs time t for fixed $\lambda = 1$ and various $K = 0$, 0.2, 0.5, and 1. To present the finite-size effects, the results for smaller 451×451 lattices (solid symbols) are also plotted for comparison. In the observed regime, they follow the power-law divergence quite well.

few percents' relative overestimation can be mostly attributed to the above-mentioned overestimation of the renormalized frequencies.

D. Mean-square displacement of the energy diffusion and the connection to the global heat current autocorrelation

Finally, we check the general relation between heat conduction and energy diffusion. It is proposed that the global heat current autocorrelation

$$C_{JJ}(t) \equiv \lim_{N\to\infty} \frac{1}{N} \langle J(t_0) J(t_0 + t) \rangle_{t_0} \tag{25}$$

is generally connected with the MSD of the spatiotemporal correlation of local energy density $\sigma^2(t)$ by [20]

$$\frac{d^2}{dt^2}\sigma^2(t) = \frac{2C_{JJ}(t)}{k_B T^2 c_v}, \tag{26}$$

where c_v denotes the specific volumetric heat capacity. Such a connection is rigorous for 1D systems with symmetric interparticle interactions and the derivations can be directly extended to 2D.

For 2D momentum-conserving nonlinear lattices, it is expected by both the renormalization group analysis and the mode-coupling theory that $C_{JJ}(t) \sim t^{-1}$, which implies a logarithmically divergent heat conductivity κ. Numerical simulations for the 2D PQ lattice well confirm it. Considering that, for the FPU-β lattice, the finite-size effects are much more serious, thus in a quite long regime $C_{JJ}(t)$ still follows a much slower decay $C_{JJ}(t) \sim t^{-0.75}$, which indicates a power-law divergence of $\kappa \sim L^{0.25}$ [23]. According to Eq. (26), the above results imply that the MSD of the energy diffusion $\sigma^2(t)$ should follow, in similar timescales and space scales, $t \ln t$ and $t^{1.25}$ for the 2D PQ and FPU-β lattices, respectively. In Fig. 6, our direct numerical calculation of $\sigma^2(t)$, which is defined in Eq. (6), is plotted. Quite surprisingly, $\sigma^2(t)$ follows a very clear power law $t^{1.35}$ for the PQ lattice, and $t^{1.5}$ for the FPU-β lattice. These power exponents are qualitatively consistent with the values 1.269 and 1.509 that are measured for the PQ and the FPU-β lattices with vector displacements [19]. However, compared with the above expectations, the numerically measured divergence of $\sigma^2(t)$ shown in Fig. 6 is much faster for both lattices. We attribute the noticeable discrepancy to the finite-size effects and still believe that in a much longer timescale and a much larger size scale the $t \ln t$ growth of $\sigma^2(t)$ would finally emerge, given the observation in Fig. 6 that all the curves are still bending down slowly. However, it is far beyond our current computational ability to confirm it.

IV. SUMMARY AND DISCUSSION

Energy diffusion in a few 2D FPU-type momentum-conserving nonlinear lattices with various linear strengths is studied via the equilibrium local energy spatiotemporal correlation. The diffusion propagator consists of a bell-shaped central heat mode and a sound mode extending with a constant speed of sound v_s. If the energy carriers are regarded as random walkers, then the evolution of the propagator can be well governed by a random-walk-with-velocity-fluctuation process, in which the duration times τ for each walk satisfy a power-law distribution $(\tau/\tau_0)^{-\mu-1}$ with $\mu \in (1, 2)$. The profile of the heat mode, including the central part and the tail, fits quite exactly a Lévy stable distribution with an index μ, where $\mu = 1.738$ and 1.834 for the PQ and the FPU-β lattices, respectively. Both values are evidently lower than 2, implying a superdiffusion. The profile of the sound mode also fits the scaling that is expected by an equilibrated setup, i.e., its height decays as $t^{-(\mu+\frac{1}{2})}$ and its dispersion grows as $t^{\frac{1}{2}}$. Because the studied lattices are representative 2D models with strong nonlinearity and total momentum conservation, we expect that the random walk can well describe the energy diffusion in a large class of 2D systems, regardless of their detailed topologies and parameters. However, the detailed properties of the random walk such as the index μ may vary and depend on the details of the systems. Since the time regime for the fitting is quite short ($\leqslant$80 or so), we are not able to draw any convincing conclusion for the long-time limit. It is also revealed that the profile of the cross section of the sound mode is apparently not single peaked. Two peaks are observed. Further in-depth studies need to be done before we can confirm its generality and make sure whether the two peaks are two separate sound modes or a part of an even more complicated structure.

We have also extended the renormalized phonon approach to the 2D lattices. By minimizing an upper bound of the free energy of a nonlinear lattice, we are able to work out an estimation of the speed of sound v_s analytically. Compared with the direct numerical measurements, there exists only a few percents' overestimation. This fact strongly supports that just as in the 1D lattice [29], phonons are still the dominant energy carriers in these 2D nonlinear lattices.

An unexpected observation also appears. The theoretical prediction is that the global heat current autocorrelation $C_{JJ}(t)$ in 2D momentum-conserving nonlinear lattices decays as t^{-1}. Our previous study has confirmed it for a 2D PQ lattice, although for a 2D FPU-β lattice the decay is slower due to the finite-size effects [23]. It is then naturally expected,

based on the general connection Eq. (26), that the MSD of the energy diffusion $\sigma^2(t)$ diverges as $t \ln t$, at least for the 2D PQ lattice. However, power-law superdiffusivity is still observed clearly in our numerical simulation, i.e., $\sigma^2(t) \sim t^\beta$ and β is noticeably greater than 1, which indicates clear discrepancies between the observation and the expectation. We have to say that the finite-size effects are very strong and robust and their influences on the energy diffusion are even much greater than on the heat conduction. The sizes of the systems for the simulations are still far from enough, thus the asymptotic behaviors cannot be well displayed. Simulations on many times larger sizes and longer timescales might be required, which is far beyond our current computation capability.

To understand the thermal transport in 2D systems is of apparent theoretical interests [40]. Recent progress in nanotechnology has also enabled us to measure experimentally the size dependence of the thermal conductivity in 2D nanoscale materials [41–44]. Our study may deepen the understanding of the energy diffusion process in high-dimensional materials and also help in fabricating the building blocks of nanoscale phononics devices [45].

ACKNOWLEDGMENTS

This work was supported by the National Natural Science Foundation of China under Grant No. 12075316, by the Beijing Natural Science Foundation through Grant No. 1192010, and by the Fundamental Research Funds for the Central Universities, and the Research Funds of Renmin University of China Grant No. 21XNLG26. Computational resources were provided by the Physical Laboratory of High Performance Computing at Renmin University of China.

APPENDIX: RENORMALIZED PHONON FREQUENCIES AND SOUND SPEED OF THE 2D NONLINEAR LATTICES

In this Appendix we extend an effective phonon approach to 2D and work out an estimation of the renormalized frequencies. The derivation basically follows the framework that is proposed in Refs. [37,46].

The renormalized Hamiltonian of the original one in Eq. (1) reads

$$H_0 = \sum_{i=1}^{N_X}\sum_{j=1}^{N_Y}\left[\frac{1}{2}\dot{u}_{i,j}^2 + \frac{\eta_{2D}^2}{2}\left(\Delta x_{i,j}^2 + \Delta y_{i,j}^2\right)\right], \tag{A1}$$

where $\Delta x_{i,j} \equiv u_{i,j} - u_{i-1,j}$ and $\Delta y_{i,j} \equiv u_{i,j} - u_{i,j-1}$. The parameters of η_{2D}, K and λ, are omitted in this Appendix for simplicity. The partition function for the renormalized 2D lattice reads

$$\begin{aligned} Z_0 &= \int e^{-\frac{1}{k_B T}H_0} d\vec{u} d\dot{\vec{u}} \\ &= \prod_{i=1}^{N_X}\prod_{j=1}^{N_Y}\iint e^{-\frac{1}{k_B T}\left[\frac{1}{2}\dot{u}_{i,j}^2 + \frac{\eta_{2D}^2}{2}\left(\Delta x_{i,j}^2 + \Delta y_{i,j}^2\right)\right]} du_{i,j} d\dot{u}_{i,j} \\ &= \left(\frac{\sqrt{2}\pi k_B T}{\eta_{2D}}\right)^N, \end{aligned} \tag{A2}$$

where $\vec{u}$ and $\dot{\vec{u}}$ are short for the products of all the coordinates and their time derivatives, respectively. $N \equiv N_X \times N_Y$ denotes the total particle number, as has been defined in the main text. The corresponding Helmholtz free energy

$$F_0 = -k_B T \ln Z_0 = -N k_B T \ln \frac{\sqrt{2}\pi k_B T}{\eta_{2D}}. \tag{A3}$$

The free energy F of the nonlinear lattice satisfies [47]

$$F \leqslant F_0 + \langle H - H_0 \rangle_{H_0}, \tag{A4}$$

where $\langle\cdot\rangle_{H_0}$ denotes the ensemble average with respect to the canonical measure $e^{-\frac{1}{k_B T}H_0}$,

$$\begin{aligned} &\langle H - H_0 \rangle_{H_0} \\ &= \frac{\int (H - H_0) d\vec{u} d\dot{\vec{u}}}{Z_0} \\ &= \sum_{i=1}^{N_X}\sum_{j=1}^{N_Y} \frac{\int \frac{K - \eta_{2D}^2}{2}\left(\Delta x_{i,j}^2 + \Delta y_{i,j}^2\right) e^{-\frac{1}{k_B T}\frac{\eta_{2D}^2}{2}\left(\Delta x_{i,j}^2 + \Delta y_{i,j}^2\right)} du_{i,j}}{\int e^{-\frac{1}{k_B T}\frac{\eta_{2D}^2}{2}\left(\Delta x_{i,j}^2 + \Delta y_{i,j}^2\right)} du_{i,j}} \\ &\quad + \sum_{i=1}^{N_X}\sum_{j=1}^{N_Y} \frac{\int \frac{\lambda}{4}\left(\Delta x_{i,j}^4 + \Delta y_{i,j}^4\right) e^{-\frac{1}{k_B T}\frac{\eta_{2D}^2}{2}\left(\Delta x_{i,j}^2 + \Delta y_{i,j}^2\right)} du_{i,j}}{\int e^{-\frac{1}{k_B T}\frac{\eta_{2D}^2}{2}\left(\Delta x_{i,j}^2 + \Delta y_{i,j}^2\right)} du_{i,j}} \\ &= \frac{N k_B T}{8\eta_{2D}^4}\left(-4\eta_{2D}^4 + 4K\eta_{2D}^2 + 3\lambda k_B T\right). \end{aligned} \tag{A5}$$

To find the value of η_{2D} that minimizes the upper bound of F, i.e., the right-hand side of Eq. (A4), let

$$\begin{aligned} &\frac{\partial\left(F_0 + \langle H - H_0 \rangle_{H_0}\right)}{\partial \eta_{2D}^2} \\ &= \frac{N k_B T}{4\eta_{2D}^6}\left(2\eta_{2D}^4 - 2K\eta_{2D}^2 - 3\lambda k_B T\right) = 0. \end{aligned} \tag{A6}$$

Then the physically relevant root

$$\eta_{2D} = \sqrt{\frac{K + \sqrt{K^2 + 6\lambda k_B T}}{2}} \tag{A7}$$

reproduces Eq. (23), in which k_B has been set to unity.

On the other hand,

$$F \geqslant F_0 + \langle H - H_0 \rangle_H, \tag{A8}$$

where $\langle\cdot\rangle_H$ denotes the ensemble average with respect to the canonical measure $e^{-\frac{1}{k_B T}H}$. By maximizing the above lower bound, i.e., $\frac{\partial\left(F_0 + \langle H - H_0\rangle_H\right)}{\partial \eta_{2D}^2} = 0$, we obtain another estimation of η_{2D}, which reads

$$\begin{aligned} \eta_{2D} &= \sqrt{\frac{N k_B T}{\sum_{i=1}^{N_X}\sum_{j=1}^{N_Y}\left\langle \Delta x_{i,j}^2 + \Delta y_{i,j}^2 \right\rangle_H}} \\ &= \sqrt{\frac{k_B T}{\left\langle \overline{\Delta x_{i,j}^2} + \overline{\Delta y_{i,j}^2} \right\rangle_H}}. \end{aligned} \tag{A9}$$

We have confirmed numerically that, similar to the case in 1D systems [37], the so obtained η_{2D} is even more accurate. However, since the result cannot be written in a closed form, it has been much less widely applied, compared with the one obtained from the upper bound of F in Eq. (A4).

[1] A. Blumen, G. Zumofen, and J. Klafter, Transport aspects in anomalous diffusion: Lévy walks, Phys. Rev. A **40**, 3964 (1989).

[2] S. Denisov, J. Klafter, and M. Urbakh, Dynamical Heat Channels, Phys. Rev. Lett. **91**, 194301 (2003).

[3] T. H. Solomon, E. R. Weeks, and H. L. Swinney, Observation of Anomalous Diffusion and Lévy Flights in a Two-Dimensional Rotating Flow, Phys. Rev. Lett. **71**, 3975 (1993).

[4] P. Cipriani, S. Denisov, and A. Politi, From Anomalous Energy Diffusion to Levy Walks and Heat Conductivity in One-Dimensional Systems, Phys. Rev. Lett. **94**, 244301 (2005).

[5] V. Zaburdaev, S. Denisov, and P. Hänggi, Perturbation Spreading in Many-Particle Systems: A Random Walk Approach, Phys. Rev. Lett. **106**, 180601 (2011); Erratum: Perturbation Spreading in Many-Particle Systems: A Random Walk Approach [Phys. Rev. Lett. **106**, 180601 (2011)], **109**, 069903(E) (2012).

[6] R. Metzler and J. Klafter, The random walk's guide to anomalous diffusion: A fractional dynamics approach, Phys. Rep. **339**, 1 (2000); A. Dhar, Heat transport in low-dimensional systems, Adv. Phys. **57**, 457 (2008).

[7] S. Lepri, Relaxation of classical many-body Hamiltonians in one dimension, Phys. Rev. E **58**, 7165 (1998); L. Delfini, S. Lepri, R. Livi, and A. Politi, Self-consistent mode-coupling approach to one-dimensional heat transport, *ibid.* **73**, 060201(R) (2006); Anomalous kinetics and transport from 1d self-consistent mode-coupling theory, J. Stat. Mech. (2007) P02007.

[8] O. Narayan and S. Ramaswamy, Anomalous Heat Conduction in One-Dimensional Momentum-Conserving Systems, Phys. Rev. Lett. **89**, 200601 (2002).

[9] R. Kubo, M. Toda, and N. Hashitsume, *Statistical Physics II*, Springer Series in Solid State Sciences Vol. 31 (Springer, Berlin, 1991).

[10] S. Lepri, R. Livi, and A. Politi, Heat Conduction in Chains of Nonlinear Oscillators, Phys. Rev. Lett. **78**, 1896 (1997).

[11] T. Hatano, Heat conduction in the diatomic Toda lattice revisited, Phys. Rev. E **59**, R1 (1999).

[12] P. Grassberger, W. Nadler, and L. Yang, Heat Conduction and Entropy Production in a One-Dimensional Hard-Particle Gas, Phys. Rev. Lett. **89**, 180601 (2002).

[13] J. M. Deutsch and O. Narayan, One-dimensional heat conductivity exponent from a random collision model, Phys. Rev. E **68**, 010201(R) (2003).

[14] L. Wang and T. Wang, Power-law divergent heat conductivity in one-dimensional momentum-conserving nonlinear lattices, Europhys. Lett. **93**, 54002 (2011).

[15] A. Kundu, C. Bernardin, K. Saito, A. Kundu, and A. Dhar, Fractional equation description of an open anomalous heat conduction set-up, J. Stat. Mech. (2019) 013205.

[16] B. Li, J. Wang, L. Wang, and G. Zhang, Anomalous heat conduction and anomalous diffusion in nonlinear lattces, single wall nanotubes, and billiard gas channels, Chaos **15**, 015121 (2005).

[17] H. van Beijeren, Exact Results for Anomalous Transport in One-Dimensional Hamiltonian Systems, Phys. Rev. Lett. **108**, 180601 (2012); C. B. Mendl and H. Spohn, Dynamic Correlators of Fermi-Pasta-Ulam Chains and Nonlinear Fluctuating Hydrodynamics, *ibid.* **111**, 230601 (2013); H. Spohn, Nonlinear fluctuating hydrodynamics for anharmonic chains, J. Stat. Phys. **154**, 1191 (2014); S. G. Das, A. Dhar, K. Saito, C. B. Mendl, and H. Spohn, Numerical test of hydrodynamic fluctuation theory in the Fermi-Pasta-Ulam chain, Phys. Rev. E **90**, 012124 (2014).

[18] The propagator, also known as the Green's function, denotes the solution of the diffusion equation for the delta-function-type initial condition.

[19] J. Wang, T.-x. Liu, X.-z. Luo, X.-L. Xu, and N. Li, Anomalous energy diffusion in two-dimensional nonlinear lattices, Phys. Rev. E **101**, 012126 (2020).

[20] S. Liu, P. Hänggi, N. Li, J. Ren, and B. Li, Anomalous Heat Diffusion, Phys. Rev. Lett. **112**, 040601 (2014).

[21] A. Lippi and R. Livi, Heat conduction in two-dimensional nonlinear lattices, J. Stat. Phys. **100**, 1147 (2000); L. Yang, P. Grassberger, and B. Hu, Dimensional crossover of heat conduction in low dimensions, Phys. Rev. E **74**, 062101 (2006).

[22] D. Xiong, J. Wang, Y. Zhang, and H. Zhao, Heat conduction in two-dimensional disk models, Phys. Rev. E **82**, 030101(R) (2010).

[23] L. Wang, B. Hu, and B. Li, Logarithmic divergent thermal conductivity in two-dimensional nonlinear lattices, Phys. Rev. E **86**, 040101(R) (2012).

[24] H. Zhao, Identifying Diffusion Processes in One-Dimensional Lattices in Thermal Equilibrium, Phys. Rev. Lett. **96**, 140602 (2006).

[25] S. Chen, Y. Zhang, J. Wang, and H. Zhao, Diffusion of heat, energy, momentum, and mass in one-dimensional systems, Phys. Rev. E **87**, 032153 (2013).

[26] The denominator of the first term on the right-hand side of Eq. (5) includes not only $C_{\mathrm{EE}}(0,0,0)$, but $C_{\mathrm{EE}}(-1,0,0)$, $C_{\mathrm{EE}}(1,0,0)$, $C_{\mathrm{EE}}(0,-1,0)$, and $C_{\mathrm{EE}}(0,1,0)$ as well, because coupled particles share the potential energy in the couplings [see the definition of $E_{ij}(t)$ in Eq. (4)], thus the latter four are also inherently nonzero.

[27] L. Wang, Z. Wu, and L. Xu, Super heat diffusion in one-dimensional momentum-conserving nonlinear lattices, Phys. Rev. E **91**, 062130 (2015).

[28] V. Zaburdaev, S. Denisov, and J. Klafter, Lévy walks, Rev. Mod. Phys. **87**, 483 (2015).

[29] N. Li, B. Li, and S. Flach, Energy Carriers in the Fermi-Pasta-Ulam β Lattice: Solitons or Phonons?, Phys. Rev. Lett. **105**, 054102 (2010).

[30] V. Zaburdaev, I. Fouxon, S. Denisov, and E. Barkai, Superdiffusive Dispersals Impart the Geometry of Underlying Random Walks, Phys. Rev. Lett. **117**, 270601 (2016).

[31] J. Klafter and I. M. Sokolov, *First Steps in Random Walks: From Tools to Applications* (Oxford University Press, Oxford, UK, 2011).

[32] J. Klafter and G. Zumofen, Dynamically generated enhanced diffusion: The stationary state case, Physica A **196**, 102 (1993).

[33] C. Alabiso, M. Casartelli, and P. Marenzoni, Nearly separable behavior of Fermi-Pasta-Ulam chains through the stochasticity threshold, J. Stat. Phys. **79**, 451 (1995).

[34] B. Gershgorin, Y. V. Lvov, and D. Cai, Interactions of renormalized waves in thermalized Fermi-Pasta-Ulam chains, Phys. Rev. E **75**, 046603 (2007).

[35] T. Dauxois, M. Peyrard, and A. R. Bishop, Dynamics and thermodynamics of a nonlinear model for DNA denaturation, Phys. Rev. E **47**, 684 (1993).

[36] D. He, S. Buyukdagli, and B. Hu, Thermal conductivity of anharmonic lattices: Effective phonons and quantum corrections, Phys. Rev. E **78**, 061103 (2008).

[37] J. Liu, S. Liu, N. Li, B. Li, and C. Wu, Renormalized phonons in nonlinear lattices: A variational approach, Phys. Rev. E **91**, 042910 (2015).

[38] Since $N_X = N_Y$, for each lattice, the lowest nonzero renormalized frequency equals $\eta_{2D}(K, \lambda)$ $\omega_{1,0}(1, 0) = \eta_{2D}(K, \lambda)\omega_{1,0}(0, 1)$, the second lowest one equals $\eta_{2D}(K, \lambda)\omega_{1,0}(1, 1)$, the third lowest one equals $\eta_{2D}(K, \lambda)\omega_{1,0}(2, 0) = \eta_{2D}(K, \lambda)\omega_{1,0}(0, 2)$, and so on.

[39] According to the nonlinear fluctuating hydrodynamic theory [17], the sound speed can be measured from the momentum correlation function even more exactly [25]. We have also done it and obtained consistent results.

[40] *Thermal Transport in Low Dimensions: From Statistical Physics to Nanoscale Heat Transfer*, edited by S. Lepri, Lecture Notes in Physics Vol. 921 (Springer, Berlin, 2016); A. Dhar, A. Kundu, and A. Kundu, Anomalous heat transport in one dimensional systems: A description using nonlocal fractional-type diffusion equation, Front. Phys. **7**, 159 (2019).

[41] S. Ghosh, W. Bao, D. L. Nika, S. Subrina, E. P. Pokatilov, C. N. Lau, and A. A. Balandin, Dimensional crossover of thermal transport in few-layer graphene, Nat. Mater. **9**, 555 (2010).

[42] Z. Wang, R. Xie, C. T. Bui, D. Liu, X. Ni, B. Li, and J. T. L. Thong, Thermal transport in suspended and supported few-layer graphene, Nano Lett. **11**, 113 (2011).

[43] D. L. Nika, A. S. Askerov, and A. A. Balandin, Anomalous size dependence of the thermal conductivity of graphene ribbons, Nano Lett. **12**, 3238 (2012).

[44] X. Gu, Y. Wei, X. Yin, B. Li, and R. Yang, *Colloquium*: Phononic thermal properties of two-dimensional materials, Rev. Mod. Phys. **90**, 041002 (2018).

[45] N. Li, J. Ren, L. Wang, G. Zhang, P. Hänggi, and B. Li, *Colloquium* : Phononics: Manipulating heat flow with electronic analogs and beyond, Rev. Mod. Phys. **84**, 1045 (2012).

[46] N. Li and J. Liu, Accessing general relations for temperature coefficients of Raman shifts in 2D materials, J. Phys.: Condens. Matter **32**, 285402 (2020).

[47] J. W. Gibbs, *Elementary Principles in Statistical Mechanics* (Longmans Green, New York, 1928).